Non-isothermal Buoyancy-Driven Exchange Flow of Miscible Fluids in inclined Pipes

A Thesis

Presented to

The Faculty of the Department of Mechanical Engineering

University of Houston

In Partial Fulfillment

of the Requirement of the Degree

Master of Science

in

Mechanical Engineering

By

Bahareh Eslami

December 2016

Non-isothermal Buoyancy-Driven Exchange Flow of Miscible Fluids in inclined Pipes

Bahareh Eslami

Approved

Chair of Committee
Hadi Ghasemi, Bill D. CookAssistant Professor
Mechanical Engineering

Committee Members:

Ralph Metcalfe, Professor
Mechanical Engineering

Kamran Alba, Assistant Professor
College of Technology

Suresh K. Khator, Associate Dean
Cullen College of Engineering

Pradeep Sharma, Professor and Chair
Mechanical Engineering

Acknowledgment

First of all, I would like to convey my sincere thanks to my supervisors Professor Kamran Alba and Professor Hadi Ghasemi for their encouragement, support, patience and invaluable suggestions that made this work successful.

I am thankful to my graduate examining committee member Professor Ralph Metcalfe for his time in reviewing this work, encouragement and insightful comments.

A very special thanks goes out to my best friends Shadi Shariatnia, Milad Yarali and Hesam Moradi for all of the unforgettable and sweet memories that we made together in Houston.

Finally, I take this opportunity to express the profound gratitude from my deep heart to my beloved parents. Thank you for all the love you gave me and the sacrifices you made for me. You are always there for me.

Non-isothermal Buoyancy-Driven Exchange Flow of Miscible Fluids in inclined Pipes

An Abstract

of a

Thesis

Presented to

The Faculty of the Department of Mechanical Engineering

University of Houston

In Partial Fulfillment

of the Requirement of the Degree

Master of Science

in

Mechanical Engineering

By

Bahareh Eslami

December 2016

Abstract

This thesis studies non-isothermal buoyancy-driven exchange flow of two miscible Newtonian fluids in an inclined pipe experimentally. The cold heavy fluid is released into the hot light one in an adiabatic small-aspect-ratio pipe in the Boussinesq limit. The maximal rate of interpenetration of the fluids in non-isothermal case is similar to the isothermal limit, maximal rate occurs at an intermediate angle. There has also been observed a novel asymmetric behavior in the flow never observed before in the isothermal limit in which the cold finger appears to advance faster than the hot one. Backed by meticulously-designed supplementary experiments, this asymmetric behavior is hypothetically associated with the wall contact and the formation of a warm less-viscous film of the fluid lubricating the cold more-viscous finger along the pipe. The asymmetric behavior of the flow is finally quantified over the full range of non-isothermal experiments carried.

Table of Contents

List of Figures

List of Tables

1. Introduction

Buoyancy-driven flow due to the release of a heavy fluid into a light one has been one of the most fundamental fluid mechanics problems found in natural context [1-4]. These flows also have many industrial applications in Counter-Current Extraction Column (CCEC) contexts [5]. CCECs are designed to remove a dispersed (contaminant) element from a heavy mixture through mixing it with a light phase containing an appropriate solvent [6]. These devices are widely used in a variety of processes and industries including chemical and municipal (organic solvents recovery, waste-water purification, water softening [7,8], biochemistry (Butanediol production [9]), pharmaceutical and biomedical (solanesol production [10]), biotechnology (protein extraction [11]), etc. The exchange flows have largely been studied in literature experimentally [13-16], computationally [19-22] and analytically [23,24] assuming fluids with equal temperature i.e., *isothermal*. The *non-isothermal* flows can be exceptionally distinct from those of isothermal as revealed in the recent computational study of [25]. However, these flows have received very little attention in literature due to the underlying complexity arising from temperature-dependent density and viscosity fields which in turn influence buoyancy, interfacial stability and fluids mixing.

Buoyant exchange flow of isothermal fluids is studied in literature using vertical [12] and inclined tubes [18, 23]. Depending on the flow parameters, *viscous*, *transitionary* and *diffusive* flows may appear. *Slumping* viscous regimes are found at nearly-horizontal angles due to strong segregative buoyancy force at the interface [17]. The interfacial instabilities grow at higher inclination angles enhancing mixing. The changeover from viscous to

transitionary flows happens at $Re_t Cos\beta \geq 50$, where $Re_t = \frac{\hat{V}_v}{\hat{V}_t}$ is a critical Reynolds number with $V_v = \frac{At\,\hat{g}\,\hat{D}^2}{v}$ and $V_t = (At\,\hat{g}\,\hat{D})^{1/2}$ being the velocity scales obtained from viscous-buoyant and inertial-buoyant stresses balance respectively [12]. Here, $\hat{\rho}$, is the average density, $\hat{\mu}$, the common viscosity of the fluids, $\hat{g}$, the gravitational acceleration and $At = \frac{\rho_H - \rho_L}{\rho_H + \rho_L}$, the Atwood number characterizing the density difference between the heavy and light fluids. In the viscous regime, the interpenetrating speed of fluids is found to be proportional to $\hat{V}_v cos\beta$. In the transitionary regime, the speed of the propagating fronts is obtained as $\hat{V}_f \approx 0.7\hat{V}_t$. The speed of the interpenetrating fronts for the diffusive regime is small, increasing slightly with the tilt angle, β, [15]. The interfacial instabilities commonly observed in multi-fluid and exchange flows may originate from a counter-current velocity profile (Kelvin-Helmholtz instability) [26-28], density contrast [29, 30], and/or viscosity contrast (Saffman-Taylor instability) [31, 32]. The heat transfer and non-isothermal effects, in fact, contribute to the flow stability/instability through modifying the fluids' density and/or viscosity contrasts [25].

Buoyant convective flow of a single fluid confined between two plates held at different temperatures has long been investigated in literature within Rayleigh-Benard (RB) context [33]. The heat transfer in the RB case is primarily controlled by the plates neighboring region due to the existing concentrated temperature gradients. This rather *localized* and *non-homogeneous* transfer of heat, however, does not relate well to many natural situations where such a confinement does not exist [34]. The exceptional idea of *homogeneous convective flows*, avoiding the effect of end plates, was first introduced in rather recent study of Giber *et al*. [34] and later led to a revolution in the field of convection; see [35,

36] and [37-39] for convection in vertical and inclined geometries respectively. As the inclination angle of the geometry is changed from vertical, different regimes namely *hard turbulent*, *soft turbulent*, *intermittent* and *laminar* may develop [37]. The transition to laminar flows occurs for $Ri > 0.05$, where Ri is the Richardson number expressing the ratio of the buoyancy term to the flow velocity gradient [38]. The flow oscillates between laminar and turbulent in the intermittent regime. See [38, 39] for recent models developed for laminar, intermittent and turbulent regimes. Through a novel experimental approach, we aim to investigate non-isothermal convective flows where the temperature difference comes from within the *bulk* of the two fluids rather than localized hot and cold regions.

The significant novelties of our study can be summarized as the followings: (i) we know of no other experimental study of non-isothermal buoyancy-driven exchange flows in the practical pipe geometry within the existing literature. Our study covers a broad range of pipe inclinations, viscosities and density differences. Various distinct flow regimes and instabilities have been identified in our study compared to the isothermal limit, all characterized in terms of the relevant flow parameters of the problem. (ii) The fundamental convection problem has been looked at from a different perspective where the temperature difference comes from within the *bulk* of the two fluids rather than localized hot and cold regions. In presenting the experimental results, we first benchmark against existing exchange flow results of isothermal fluids and then discuss the main qualitative features of the non-isothermal flows through flow visualization and Ultrasonic Doppler Velocimetry (UDV).

2. Experimental methodology

2.1 Experimental setup

Our experiments have been carried out in a 2-m long, two-fluid apparatus as shown schematically in **Fig. 1**. The pipe is made of optically-clear polycarbonate with diameter 9.5 mm resulting in a small aspect ratio of $\delta \approx 0.0048$ to capture the long time effects in non-isothermal exchange flows. For simplicity, we intended to study an adiabatic flow by choosing polycarbonate for solid boundary with low thermal conductivity ($\widehat{K}_s \approx 0.19\ W/(m.K)$. The entire pipe system is enclosed in a vacuum duct ($\approx -101\ kPa$ gauge pressure) made of acrylic to minimize the heat loss *radially*. The tube ends are connected to hot and cold reservoirs (40 L volume) via hosing and valves. Note that the convection between the two fluids in our experiments is dominant over the *circumferential* and *axial* conduction components within the solid which are minimized by choosing the smallest thickness of the pipe possible. We have further evaluated the axial conduction in the wall of the tube through solving transient heat equations in COMSOL.

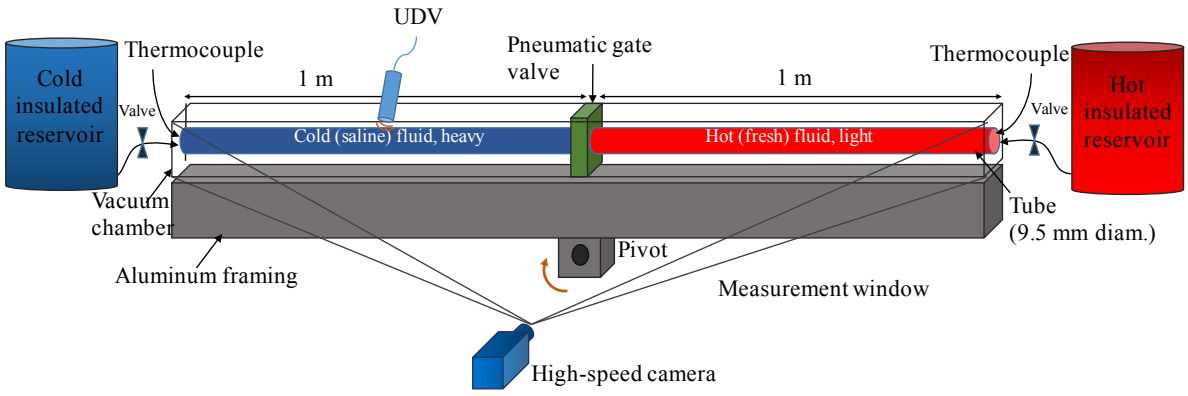

Figure 1. Schematic of the experimental set-up used in studying the buoyancy-driven exchange flow of two non-isothermal fluids in a pipe. The entire system may be tilted at an angle, β, measured from vertical.

The initial conditions were set to be uniform temperature (cold and hot) within each side of the tube. The boundary conditions were prescribed reservoir temperatures. It is found that the heat flux along the tube wall is less than 7% of that happening within the fluids. For the pair fluids, we cover a range of Newtonian fluids including, water, salt-water and glycerin-water away from their *density-inversion* temperature [40]. An advanced rheometry equipment (TA Instruments HR-3 Discovery Hybrid rheometer) is used to characterize the fluids. The viscosity of the solutions can be measured over a broad range of temperatures, thanks to Peltier temperature-control system connected to the rheometer. The viscosity of our water-based solutions vary with temperature as exponential model

$$\hat{\mu} = \hat{\mu}_0 e^{-\sigma(\hat{T}-\hat{T}_0)/\hat{T}_0}, \quad (1)$$

where $\hat{\mu}_0$ is reference viscosity of the fluid at room temperature, $\hat{T}_0 \approx 25℃$, and σ is an activation energy parameter [41]. The density of the fluids is precisely read by DMA 35 density meter from Anton Paar (0.1 kg/m^3 resolution). The fluids' coefficients of specific heat, $\hat{c}$, thermal conductivity, $\hat{k}$, and thermal expansion, $\hat{\lambda}$, are close for the pair fluids considered and are obtained using standard textbooks. The flow loop will be partially filled with the hot (light) and cold (heavy) fluids. The fluids are initially separated via a gate valve (VAT Inc.) which is operated pneumatically at $205\ kPa$.

The stainless steel hot fluid tank (drum) is equipped with an adjustable steel band heater (1500 Watts, 15-120℃) to obtain desired temperature. It has also been isolated using fiberglass insulation (EcoTouch PINK R-13, 8.9-cm thickness). The PVC cold fluid tank is also slightly heated above the room temperature using a silicone-rubber drum band heater (200 Watts, 10.2-cm wide). All the hosing and connections attached to the tanks and main pipe system have been insulated by foam wraps (0.32-cm thickness) to minimize the

slightest heat loss prior and during the experiments. Due to the small aspect ratio of the pipe, the natural convection within each side of the duct prior to the start of the experiment is negligible, even in strictly vertical position; the Rayleigh number, $Ra \approx O(10^3)$, is much less than the critical value, $Ra_{cr} \approx O(10^{11})$, predicted in [42]. This has also been validated against velocimetry measurements to be explained later. The procedure is designed so that a sharp temperature gradient across the gate is obtained prior to the experiments, i.e. cold/hot fluids on the left/right hand sides of the valve respectively. We have further confirmed this by looking into the axial heat diffusion equation

$$\frac{\partial \hat{T}}{\partial \hat{t}} = \hat{\alpha} \frac{\partial^2 \hat{T}}{\partial \hat{x}^2} . \tag{2}$$

Here, $\hat{T}$ is the temperature, $\hat{\alpha} = \hat{k}/(\hat{\rho}_0 \hat{c})$ is the thermal diffusivity and $\hat{t}$ and $\hat{x}$ are time and stream-wise distance respectively. Note that $\hat{k}$ is the fluids' common thermal conductivity and $\hat{\rho}_0$ is the initial mean density of the fluids. Assuming that the cold heavy and hot light fluids initially have temperatures $\hat{T}_{H,0}$ and $\hat{T}_{L,0}$ respectively, the solution of equation (2) can then be found in the following form:

$$\hat{T} = \hat{T}_{H,0} + \frac{\Delta \hat{T}_0}{2} \, erfc \left(\frac{\hat{x}}{2\sqrt{\hat{\alpha}\hat{t}}} \right) . \tag{3}$$

Figure 2 shows the variation of the temperature over the entire domain length, $\hat{x}$, based on (3) up to 60 s which is well beyond our experiment preparation time. A thermal diffusivity close to that of water has been used in generating the results mimicking our experiments ($\alpha \approx 1.4\times10^{-7}\ m^2/s$). It can be clearly seen that the sharp-temperature-gradient assumption made prior to the start of the experiment, for a maximal temperature gradient of $\Delta \hat{T}_0 = 50$℃, is quite fair as only a small area in the vicinity of the gate valve (-3 $cm \leq \hat{x} \leq 3\ cm$) is influenced by thermal diffusion effects. The temperature of the fluids at both

ends of the pipe is accurately monitored over time using dual thermocouples connected to a recorder (ISD-TC, Omega Engineering Inc.). Ideally, in an infinitely long tube, the end temperatures will not be affected by axial heat diffusion occurring within the domain. However, due to the laboratory limitations on the length of the pipe we notice a slight drop in the temperature of the hot fluid over time. The experiments are stopped at a stage where the error in the Atwood number due to this temperature drop exceeds 7%.

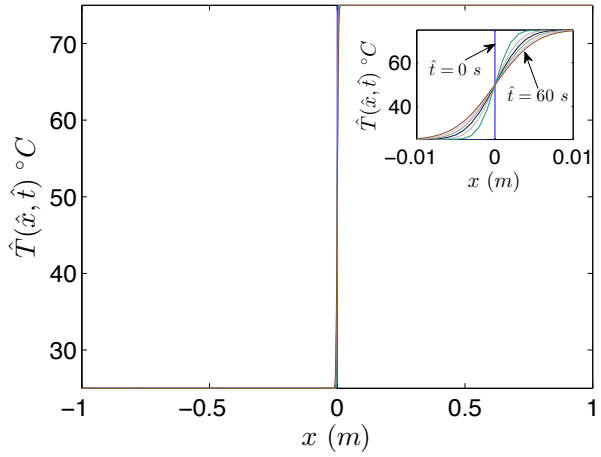

Figure 2. Variation of the temperature, $\hat{T}$, with distance, $\hat{x}$, and time, $\hat{t}$, based on the solution of (3) using $\hat{T}_{H,0}$ =20℃, $\Delta\hat{T}_0$ =60 ℃ and $\hat{\alpha}$≈1.4×10^{-7} m^2/s. A negligible distance of maximum 0:08 m on each side of the gate valve seems to have been affected by thermal diffusion prior to the experiments

Black dye (ink) with concentration 900 *mg/L* is added to the displacing fluid in order to measure concentration via optical absorption (Beer-Lambert law). The low concentration of the dye used does not change the fluid properties. The pipe is back-lit using Light-Emitting Diode (LED) strips. A diffusive layer is placed between LED strips and pipe to improve light homogeneity. The optical measurement method consists of acquiring images of the pipe using a high-speed black-and-white digital camera (Basler Ace acA2040-90um CMOS, 2048^2 pixels), with $2^{12}(= 4096)$ gray-scale levels. This allows us to analyze a reasonably wide range of concentrations. The camera covers the

whole 2-m length of the pipe using a high resolution lens (16 *mm* F/1.8 C-mount) and records images at a rate of 8. Note that the black-and-white maps obtained from the camera have been converted to color pictures using a Matlab image processing code for improved presentation of the results**.**

An Ultrasonic Doppler Velocimeter (UDV), has also been used in order to measure local velocity profiles of the flow. At the start of each experiment, the gate valve is opened letting the heavy cold (saline) fluid penetrate through the light hot (fresh) one due to gravity. In a typical experimental sequence, we would fix the temperature (and salinity) of the fluids and run a number of experiments at various inclination angles. The repeatability of experiments have been successfully checked over various inclination angles ($\beta = 30°, 60°$) and density differences ($At_0 = 0.01$).

2.2 Range of Dimensional and Dimensionless Parameters

The geometric dimensionless parameters are namely tube inclination, β, measured from vertical, and aspect ratio, $\delta = \frac{D}{L}$. Note that in this study the dimensional quantities are denoted with ^ symbol e.g. the tube diameter is $\widehat{D}$, and dimensionless quantities without. The dimensionless temperature difference ratio is denoted by $r_T = \frac{\Delta\hat{T}_0}{\hat{T}_{H,0}}$. The Atwood number, based on the fluids initial densities, is defined as $At_0 = \frac{\Delta\hat{\rho}_0}{2\hat{\rho}_0}$, representing a dimensionless density difference, where $\Delta\hat{\rho}_0 = \left(\hat{\rho}_{H,0} - \hat{\rho}_{L,0}\right)$ and $\hat{\rho}_0 = \frac{\hat{\rho}_{H,0}+\hat{\rho}_{L,0}}{2}$ are the density difference and the mean density respectively. Our focus in this study is on small At_0, the significance of which is that a *Boussinesq* approximation is valid [43]. Briefly, this means that density differences can significantly affect the buoyancy force but not the acceleration of individual fluids. The effects of thermal expansion of the fluids on driving

buoyancy force is retained in the Grashof number defined as $Gr = \hat{g}\hat{\lambda}\Delta\hat{T}_0\hat{D}^3/v^2$. Here, $\hat{D}$ is the pipe diameter, $\hat{g}$, the gravitational acceleration and $\hat{v}$, the kinematic viscosity defined using the mean density, $\hat{\rho}_0$, and the viscosity of the heavy fluid, $\hat{\mu}_{H,0}$. Another dimensionless parameter is the Reynolds number defined as, $Re_t = \hat{V}_t\hat{D}/\hat{v}$, where $\hat{V}_t = (At_0\,\hat{g}\hat{D})^{1/2}$ is a velocity scale obtained from the balance of the buoyant, $\Delta\hat{\rho}_0\hat{g}\hat{D}$, and inertial, $\hat{\rho}_0\hat{V}^2$, stresses [16]. The viscosity ratio is denoted by $m = \hat{\mu}_{L,0}/\hat{\mu}_{H,0}$. The effect of viscosity dependency on temperature is captured in the Nahme number defined as $Na = \sigma\hat{\mu}_{H,0}\hat{V}_t^{\,2}/(\hat{k}_{H0}\hat{T}_{H,0})$, where σ is an activation energy parameter [41]. The ratio of viscous to thermal diffusivity in our convective flow is captured through the Prandtl number defined as $Pr = \hat{v}/\hat{\alpha}$. The degree of molecular diffusive transport compared to advective transport is governed by the Peclet number, $Pe = \frac{\hat{V}_t\hat{D}}{\hat{D}_m}$, where $\hat{D}_m$ is the molecular diffusion which in our study is of $O(10^{-9})\ m^2/s$. Note that due to the choice of fluids and range of temperature differences considered, viscous dissipation effects captured via the Brinkman number, $Br = \hat{\mu}_{H,0}\hat{V}_t^{\,2}/\hat{k}\Delta\hat{T}_0$, are negligible ($Br \ll 1$). A final note here is that other relevant dimensionless numbers such as Rayleigh number, Ra, Nusselt number, Nu, and Eckert number, Ec, can be constructed as a function of those represented above as $Ra = Gr.Pr$, $Nu = f(Re, Pr)$, and $Ec = Br/Pr$ respectively.

In summary, the *independent* input parameters of the problem are β, $\hat{g}$, $\hat{D}$, $\hat{L}$, $\hat{c}$, $\hat{\lambda}$, $\hat{k}$, $\hat{T}_{H,0}$, $\hat{T}_{L,0}$, $\hat{\rho}_{H,0}$, $\hat{\rho}_{L,0}$, $\hat{\mu}_{H,0}$, $\hat{\mu}_{L,0}$, $\hat{D}_m$ and σ. In the *dimensionless* space, these parameters reduce to β, δ, r_T, At_0 , Gr, Re, m, Na, Pr, Pe and Br. The ranges of dimensional and dimensionless numbers governing the flow are listed in Tables 1 and 2 along with the range considered. Evidently, we are able to cover a wide range of dimensional and dimensionless

parameters with our experiments. A total of 123 experiments have been carried (88 non-isothermal tests plus 35 benchmarking tests in isothermal limit). In presentation of our results, both dimensional and dimensionless quantities are conveniently provided. The former enable other researchers recreate the findings of this paper for benchmarking purposes etc. while the latter extend the applicability of the results via dimensional analysis to systems of different sizes, temperature, fluids phases than those used in our experimental study.

Table 1. List of dimensional independent input parameters of the problem.

Parameter	Range
$\boldsymbol{\beta}$	$\mathbf{0-90^{\circ}}$
$\hat{\mathbf{g}}$	$\mathbf{9.8\ m/s^2}$
$\hat{\mathbf{D}}$	$\mathbf{9.53\ mm}$
$\hat{\mathbf{L}}$	$\mathbf{2\ m}$
$\hat{\mathbf{c}}$	$\mathbf{4.18\ kJ/(kg.K)}$
$\hat{\boldsymbol{\lambda}}$	$\mathbf{0.0002-0.0005\ 1/K}$
$\hat{\boldsymbol{\kappa}}$	$\mathbf{0.28,\ 0.58\ W/(m.K)}$
$\hat{\mathbf{T}}_{\mathbf{H,0}}$	$\mathbf{22}^{\circ}\mathbf{C}$
$\hat{\mathbf{T}}_{\mathbf{L,0}}$	$\mathbf{40-75}^{\circ}\mathbf{C}$
$\hat{\boldsymbol{\rho}}_{\mathbf{H,0}}$	$\mathbf{998\ kg/m^3}$
$\hat{\boldsymbol{\rho}}_{\mathbf{L,0}}$	$\mathbf{960\ kg/m^3}$
$\hat{\boldsymbol{\mu}}_{\mathbf{H,0}}$	$\mathbf{0.001\ Pa.s}$
$\hat{\boldsymbol{\mu}}_{\mathbf{L,0}}$	$\mathbf{0.0005\ Pa.s}$
$\hat{\mathbf{D}}_{\mathbf{m}}$	$\mathbf{10^{-9}-10^{-11}\ m^2/s}$

Table 2. List of dimensionless independent input parameters of the problem.

Parameter	*Range*
β	$0 - 90°$
$\delta = \frac{\hat{D}}{\hat{L}}$	≈ 0.0048
$r_T = \frac{\Delta\hat{T}_0}{\hat{T}_{H,0}}$	$r_T \approx O(1)$
$At_0 = \frac{\Delta\hat{\rho}_0}{2\hat{\rho}_0}$	$0.0035,\ 0.01$
$Gr = \hat{g}\hat{\lambda}\Delta\hat{T}_0\hat{D}^3/\nu^2$	$0 \leq Gr \leq 388604$
$Re = \hat{V}_t\hat{D}/\hat{\nu}$	$34.7 \leq Re \leq 758$
$m = \hat{\mu}_{L,0}/\hat{\mu}_{H,0}$	$0.5,\ 1,\ 2$
σ	$5.522 - 20.87$
$Na = \sigma\hat{\mu}_{H,0}\hat{V}_t^{\,2}/(\hat{k}_{H0}\hat{T}_{H,0})$	$Na < 1$
$Pr = \hat{\nu}/\hat{\alpha}$	$Pr \approx O(1)$
$Pe = \frac{\hat{V}_t\hat{D}}{\hat{D}_m}$	$Pe \gg 1$
$Br = \hat{\mu}_{H,0}\hat{V}_t^{\,2}/\hat{k}\Delta\hat{T}_0$	$Br \ll 1$

2.3 Ultrasonic Doppler Velocimetry (UDV)

To gain additional insight into the dynamics of the flow, we have measured the velocity profile 500 mm downstream of the gate valve using an Ultrasonic Doppler Velocimeter (UDV) (model DOP4000 from Signal Processing SA). For the tracer, Polyamid Seeding Particles (PSP) with a mean particle diameter of 50 μm and density close to that of pair fluids ($\hat{\rho}_{PSP} = 1030\ kg/m^3$) are used to ensure they stay neutrally buoyant within the flow. A volumetric PSP concentration of 2 g/L has been added to the fluids. The measuring volume of the probe has a cylindrical shape. The axial resolution of

UDV within the depth of our fluids is about 0.128 *mm* and the lateral resolution is equal to the transducer diameter (8 *mm*), slightly varying with depth. A 4-*MHz* transducer has been used in our measurements. The UDV probe was mounted at an angle $\approx 85°$ relative to the axis of the pipe, selected to balance a good signal to noise ratio with a small ultrasonic signal reflection; see [44] for details. The method is non-intrusive as the probe is mounted outside the pipe, with the ultrasonic beam entering the fluid by passing through a 1.6 *mm*-thick polycarbonate pipe wall. Note that the area around the UDV probe is sealed so that it does not compromise the vacuum within the acrylic box surrounding the tube (**Fig. 1**). The method measures the flow velocity projection on the ultrasound beam, essentially giving the axial velocity across the pipe.

In order to increase the viscosity of the heavy fluid, a small amount of xanthan powder is added to cold water. By adding 195 and 245 *mg/L* one obtains $\hat{\mu}_{H,0} = 0.002, 0.005\ Pa.s$ respectively. Upon rheological characterization (using HR-3 Discovery Hybrid rheometer from TA Instruments) it was found that the shear-thinning effects associated with xanthan gum for the concentration given and our range of shear rate ($\hat{\dot{\gamma}} \in [0, 3]$ *1/s*) are negligible.

3. Results

We first give a broad phenomenological description of the main features we have observed in our non-isothermal experiments in section 3.1. We have also benchmarked against existing results for isothermal fluids of [16, 45]. The variations in measured advancing front velocities, important in estimating the fluids spreading rate, is studied in section 3.2. The asymmetrical effects observed in association with non-isothermal flows are investigated in depth in section 3.3. In section 3.4, we quantify the flow asymmetry over the whole range of our non-isothermal flows.

3.1 Buoyancy-driven exchange flows: benchmarking and main qualitative features

We first aim to present a typical buoyancy-driven exchange flow experiment in an inclined pipe. **Figures 3(a)** and **(b)** show snapshots of experiments carried using water-based solutions for isothermal and non-isothermal cases respectively for $\beta = 60°$ and $At = 0.01$. The fluids are initially separated by a gate valve (green rectangle) in the center. The interpenetration of heavy and light layers due to buoyancy is evident. The heavy and light fingers are mostly symmetrical in the isothermal case (**Fig. 3(a)**) as previously noted by [16]. Note that the flow in this case is solely driven by added salinity (sodium chloride, NaCl) in the heavy side. The interface between the two fluids has been destabilized due to the counter-current and Kelvin-Helmholtz type instabilities. It is interestingly observed that the flow symmetry vanishes in the presence of a temperature difference between the two fluids (**Fig. 3(b)**). Note that the flow in this case is driven through a temperature difference rather than added salinity. The heavier cold fluid layer advances faster than the light hot one. Moreover, the instabilities appear to be of different nature in the non-isothermal case. The fingers are more diffuse (at least within the cold layer) noted by the mixed

concentration values (c ≈ 0.5). Note that although the spreading speeds of the heavy and light layers are different in non-isothermal case, the net amount of mass displaced on each side of the pipe is still zero due to the conservation of mass. In other words, the heavy finger is faster but overall thinner than the light one. In order to ensure that the flow asymmetry is not an artifact due to the set-up, we switched hot and cold fluid sides recovering exactly the same results.

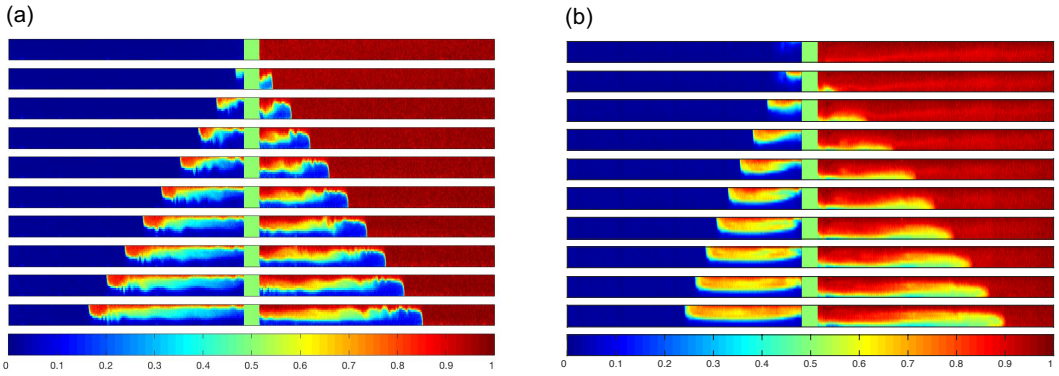

Figure 3. Snapshots of the exchange flow carried for $\beta = 60°$: (a) Isothermal study, $\hat{\rho}_{H,0} = 1017.7\ Kg/m^3$, $\hat{\rho}_{L,0} = 997.5\ Kg/m^3$ $(At = 0.01,\ Re = 372, m = 1,\ Pe = 291506)$. (b) Non-isothermal study, $\hat{T}_{H,0} = 26.7$ ℃, $\hat{T}_{L,0} = 71.7$ ℃, $\hat{\rho}_{H,0} = 997\ Kg/m^3$, $\hat{\rho}_{L,0} = 977.2\ Kg/m^3$, $(At = 0.01)$ at times $\hat{t} = [0,\ 3.33,\ 6.66,\ \ldots, 26.67,\ 30.0]\ s$.

Let us now see how the non-isothermal experiments compare against the isothermal ones over a large range of inclination angles. **Figure 4(a)** shows the snapshots of experiments carried for water based isothermal fluids revealing viscous (β = 80°), transitionary (β = 45°, 60°, 70°) and diffusive (β = 0°, 30°) flows. The degree of the instability and mixing increases as moving towards vertical. The results are in agreement with the picture provided in [17]. **Figure 4(b)** shows snapshots of non-isothermal flows obtained upon releasing heavy cold (fresh) water into light hot (fresh) one revealing completely different flows compared to the isothermal limit. It can be seen that the heavy and light fingers are overall more destabilized and diffused compared to the isothermal

case. The flow asymmetry introduced in **Fig. 3(b)** also persists over the full range of inclination angle, β.

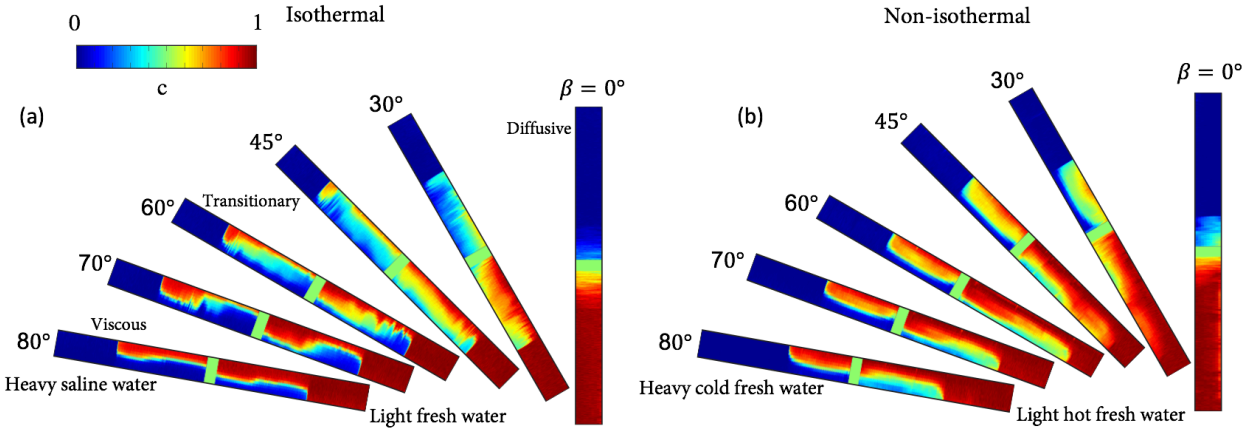

Figure 4. (a) Change in isothermal exchange flow with β, $\hat{\rho}_{H,0} = 1017.7\ Kg/m^3$, $\hat{\rho}_{L,0} = 997.5\ Kg/m^3$, at time $\hat{t} = 30.0\ s$. ($At = 0.01,\ Re = 372,\ Pe = 291506$). (b) Non-isothermal exchange flow, $\hat{T}_{H,0} = 26.7$ ℃, $\hat{T}_{L,0} = 71.7$ ℃, $\hat{\rho}_{H,0} = 997\ Kg/m^3$, $\hat{\rho}_{L,0} = 977.2\ Kg/m^3$, $\hat{\mu}_{H,0} = 8.6\times 10^{-4}\ Pa.s$, $\hat{\mu}_{L,0} = 3.9\times 10^{-4}\ Pa.s$, at time $\hat{t} = 30.0\ s$.

Before further presenting the non-isothermal experimental results, we need to ensure the accuracy of our flow loop at both qualitative and quantitative levels. Detailed benchmarking tests against [27–29] have been carried out in this regard. We have run 35 experiments using isothermal fluids covering β = 0−90° and At = 0.0035,0.01,0.04 ($Re =$ [170,600]). The validity of these experiments have been checked using four ways: 1) Seon et al. [16] classified various viscous, transitionary and diffusive regimes using the dimensionless controlling parameter Re cosβ. The parameter Re cosβ represents the relative strength of the stream-wise buoyant $(\hat{\rho}_H - \hat{\rho}_L)\hat{g}cos\beta\hat{D}$, to viscous $\hat{\mu}V_t/\hat{D}$ stresses [90]. Seon et al. [16] found that the changeover from viscous to transitionary flows happens at $Re_t Cos\beta \geq 50$. **Figure 5** obtained from our isothermal benchmarking experiments does confirm such transition. Note that various colors in **Fig. 5** correspond to different Atwood

numbers. 2) The frontal speed of the advancing heavy and light fingers in the case of viscous flows is reported to obey $\hat{V}_f = (\frac{1}{16} - \frac{1}{2\pi^2})\hat{V}_v cos\beta$Vˆ i.e., $\frac{\hat{V}_f}{\hat{V}_t} = (\frac{1}{16} - \frac{1}{2\pi^2})Re_t cos\beta$ [16]. Our scaled front velocity measurements, $\frac{\hat{V}_f}{\hat{V}_t}$, for viscous flows accompanied by error bars show close agreement with this prediction which is indicated by a dashed line in **Fig. 5**. 3) Seon et al [16] further revealed that the frontal speed in transitionary flows mostly converges to $\frac{\hat{V}_f}{\hat{V}_t} \approx 0.7$. Our results for transitionary flows closely follow such prediction which has been highlighted by a solid line in **Fig. 5**. 4) The heavy and light fluids interpenetrating speed in the case of diffusive flows is low due to strong transverse mixing [16].

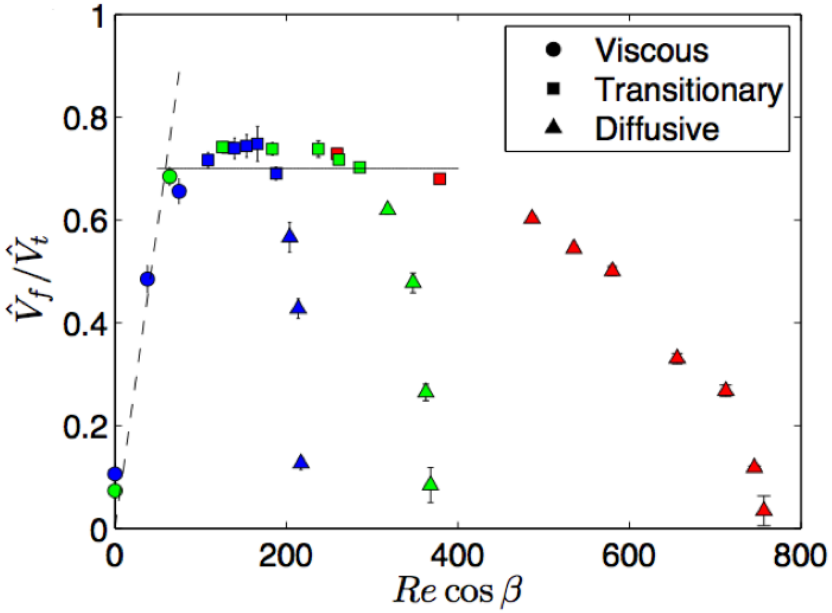

Figure 5. (a) Classification of our benchmarking tests for isothermal experiments presented in $(\frac{\hat{V}_f}{\hat{V}_t}, Re_t Cos\beta)$ −Plane: Viscous regime (●), intermittent regime (■), fully diffusive regime (▲). (b) Variation of the dimensionless macroscopic diffusion coefficient versus tilt angle. The crosses are based on our measurements for $At = 0.04$, triangles for $At = 0.01$ and squares for $At = 0.0035$.

The depth-averaged concentration $\overline{C}\,(\hat{x},\hat{t})$ may not give any information whether or not the flow is symmetric in the transverse direction. However, it does provide us with some very useful information about how much heavy and/or light fluids exist in a given stream-wise location, $\hat{x}$, at time $\hat{t}$. **Figure 6** shows the spatiotemporal diagrams of the depth-averaged concentration field, $\overline{C}\,(\hat{x},\hat{t})$, for the same non-isothermal experiments as shown in **Fig. 4(b)**. The green region in the vicinity of $\hat{x} = 0\ mm$ corresponds to the gate valve. The flow asymmetry effect is evident from spatiotemporal diagrams i.e. increased flow advancement on the right-hand-side area of the gate valve ($\hat{x} > 0$). It can also be interestingly observed that slope of the spatiotemporal diagram corresponding to the heavy and light fronts show a non-linear behaviour at short times (small $\hat{t}$) which is later reduced. This non-linear behavior is due to initial buoyant-inertial balance as explained in [22]. At longer times, the dynamics of the flow is dictated by buoyant-viscous balance identified by semi-linear region in spatiotemporal diagrams. Also note the unsteadiness in spatiotemporal diagrams due to the propagation of interfacial waves specially for inclinations away from horizontal (β = 0°, 30°,45° cases in **Fig. 6**). Another comment to make here is that the boundary between heavy and light fluids in spatiotemporal diagram is less clear for highly mixing flows (see for instance β = 0°, 30° cases in **Fig. 6**) due to the diffuse nature of these flows. When the degree of interfacial mixing is reduced, it is easier to spot the border of heavy and light fluids as depicted in β = 60°, 70°, 80° examples in **Fig. 6**.

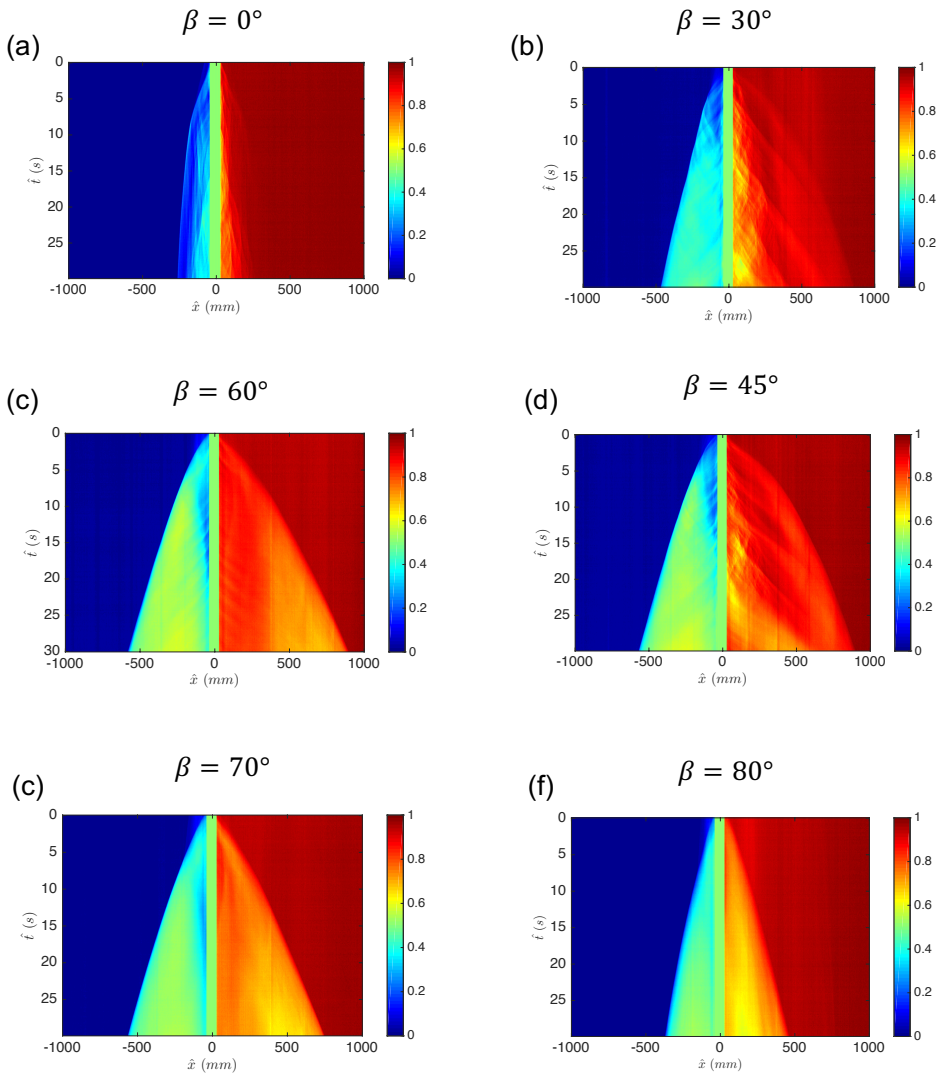

Figure 6. Spatiotemporal diagrams of depth-averaged concentration field, $\bar{C}_{\hat{y}}(\hat{x},\hat{t})$, for the same experiments as shown in Spatiotemporal (a) $\beta = 0°$, (b) $\beta = 30°$, (c) $\beta = 45°$, (d) $\beta = 60°$, (e) $\beta = 70°$, (f) $\beta = 80°$.

3.2 Front velocity measurement and characteristics

The buoyancy force originating from fluids' density difference continuously drives the interpenetrating flow in question along the stream-wise direction, meanwhile segregating the phases in the depth-wise direction. Depending on the driving and segregative buoyant components as well as flow instability, the interpenetration of two fluids may be slow and/or fast. It is critical to quantify the spreading speed of

interpenetrating layers in the case of non-isothermal fluids specially when designing well cementing and/or counter-current extraction column processes. The front velocity can be measured via tracking the depth-averaged concentration profile, $\overline{C}\,(\hat{x},\hat{t})$, over time. **Figure 7(a)** depicts the evolution of $\overline{C}\,(\hat{x},\hat{t})$ over space, $\hat{x}$, at different times $\hat{t}$ = [0,3.33,6.66,...,26.67,30.0] s, for a typical experiment shown in Fig. 3b. By closely following $\overline{C} > 0$ ($\overline{C} < 1$) one will be able to realize the entrance of light (heavy) fluid at location $\hat{x}$. To avoid the noise in the data close to the lower wall of the pipe, we estimate the speed of the heavy and light fingers by the velocity of the concentration levels $\overline{C}$ = 0.1,0.9 respectively (see the solid and dashed lines in **Fig. 7(a)**).

Figure 7(b) shows the variation of the heavy and light fingers velocities, $\hat{V}_{f,H}$ and $\hat{V}_{f,L}$ respectively, with time, which is quite typical of most of our experiments. After opening the gate valve at $\hat{t}$ = 0 the velocities abruptly increase from 0 (stationary flow) but relax back to steady levels, at longer times. See also [46] for analogous behavior witnessed in other similar gravity currents. For the case depicted, $\hat{V}_{f,H}$ = 29.3 mm/s and $\hat{V}_{f,L}$ = 17.3 mm/s at long times (15 s $\leq \hat{t} \leq$ 30 s). In practice, it is the longtime front velocity (away from the initial transients) that we are interested to study. Studying the transient/short-time effects in exchange flows can be interesting but is beyond the scope of our study. The heavy fluid advancing front velocity seems to be consistently larger than that of the light fluid confirming the asymmetry. The selection of a threshold value is evidently a trade-off between robustness and proximity to $\overline{C}$ = 0,1. In order to ensure the validity of the technique, the $\hat{V}_{f,H}$ and $\hat{V}_{f,L}$ readings have also been compared upon the slope of the spatiotemporal diagram. Values of $\hat{V}_{f,H}$ = 29.8 mm/s and $\hat{V}_{f,L}$ = 18.6 mm/s have correspondingly been obtained showing close agreement with the threshold method. Note

that the advantage of the threshold method over slope of spatiotemporal diagram is that the former works for all viscous/transitionary/diffusive regimes whereas the latter fails in the case of diffusive regime; see [44, 47] for more details on front velocity measurement.

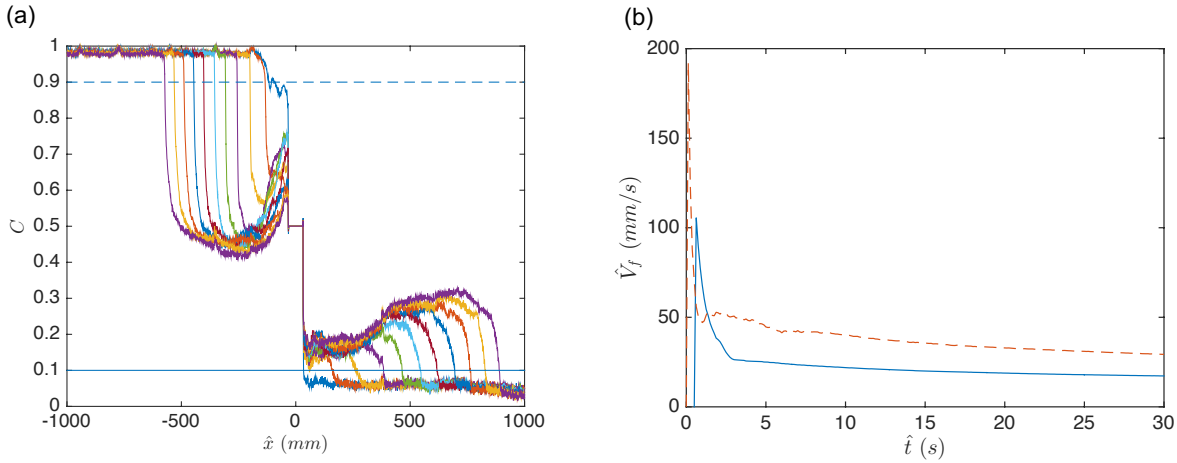

Figure 7. Velocity Reading: (a) Evolution of the depth-averaged concentration field, $\bar{C}_{\hat{y}}(\hat{x},\hat{t})$, with time, $\hat{t} = [0,\ 3.33,\ 6.66,\ \ldots, 26.67,\ 30.0]\ s$, and streamwise location, $\hat{x}$, measured from the gate valve for the same experiment as in Fig. Isothermal vs Nonisothermal (b).

We now explore the main characteristics of front velocity measurements across our experimental range, where we have varied inclination angles, β, and density differences, At. Note that in terms of the process design, both the heavy and light fingers speeds, $\hat{V}_{f,H}$ and $\hat{V}_{f,L}$, are of importance. **Figures 8(a)** and **(b)** show $\hat{V}_{f,H}$ and $\hat{V}_{f,L}$ respectively for non-isothermal experiments over various inclination angles, β, and At = 0.0035,0.01. Firstly, note that the values of both the heavy and light front velocities increase with the density difference (Atwood number) over almost all range of β. This is due to the fact that the driving force of the flow from buoyancy naturally increases with At resulting in higher fluids interpenetration rate. The counter-current buoyant stress acts as $(\hat{\rho}_H - \hat{\rho}_L)\ \hat{g}\cos\beta$ (note that $(\hat{\rho}_H - \hat{\rho}_L)\ \hat{g}\sin\beta$ acts to segregate the layers depth-wise) which is maximum at β = 0° . One would then expect $\hat{V}_{f,H}$ and $\hat{V}_{f,L}$ to be the highest close to this angle. However, from

Fig. 8, it can be seen that at a given Atwood number, At, the front velocity roughly seems to be the highest for an intermediate inclination angle between vertical (β = 0°) and horizontal (β = 90°) extremes. Rooted in Boycott-type effect [16], the counter-current flow is strong enough in this range to increase the frontal speeds but not to an extent to promote interfacial instabilities (of mainly Kelvin-Helmholtz nature) which in turn tend to decrease the speeds. Lastly, upon comparing **Figs. 8(a)** and **(b)**, note that $\hat{V}_{f,H}$ values are consistently higher than $\hat{V}_{f,L}$ confirming flow asymmetry using a different presentation than flow snapshot (Fig. 4) and/or spatiotemporal diagram (**Fig. 6**).

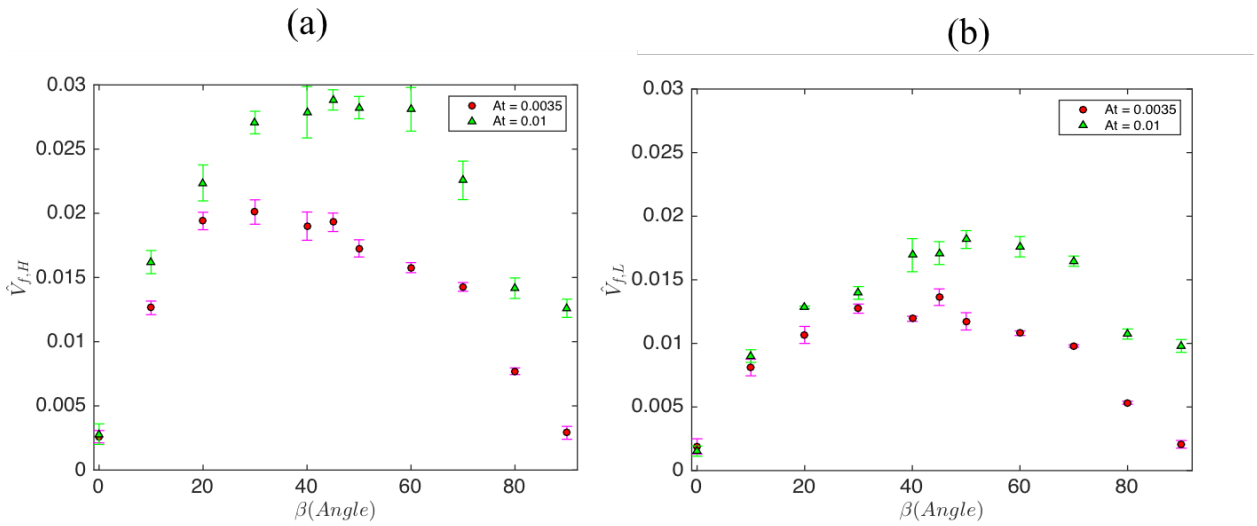

Figure 8. Change in (a) heavy front velocity, $\hat{V}_{f,H}$, and (b) light front velocity, $\hat{V}_{f,L}$, with tilt angle, β. Different markers represent $At = 0.0035$ (●), 0.01 (Δ). The dashed lines are guide to the eye

To gain additional insight into the dynamics of the flow, we have measured the velocity profile 500 mm downstream of the gate valve using an Ultrasonic Doppler Velocimeter (UDV) (model DOP4000 from Signal Processing SA). For the tracer, Polyamid Seeding Particles (PSP) with a mean particle diameter of 50 μm and density close to that of pair fluids ($\hat{\rho}_{PSP}$= 1030 kg/m^3) are used to ensure they stay neutrally buoyant within the flow. A volumetric PSP concentration of 2 g/L has been added to the fluids. The

measuring volume of the probe has a cylindrical shape. The axial resolution of UDV within the depth of our fluids is about 0.128 mm and the lateral resolution is equal to the transducer diameter (8 mm), slightly varying with depth. A 4 − MHz transducer has been used in our measurements. The UDV probe was mounted at an angle ≈ 85° relative to the axis of the pipe, selected to balance a good signal to noise ratio with a small ultrasonic signal reflections; see [93] for details. The method is non-intrusive as the probe is mounted outside the pipe, with the ultrasonic beam entering the fluid by passing through a 1.6 mm-thick polycarbonate pipe wall. Note that the area around the UDV probe is sealed so that it does not compromise the vacuum within the acrylic box surrounding the tube (**Fig. 1**). The method measures the flow velocity projection on the ultrasound beam, essentially giving the axial velocity across the pipe.

In **Fig. 9** flow dynamics of a non-isothermal experiment have been studied. In **Fig. 9(b)** zero velocity has been recorded, since the flow has not reached the UDV probe. Part **(c)** and **(d)** indicate the velocity measurements when finger is passing below the probe and while the tip of the finger has passed, respectively.

3.3 Investigating the asymmetry effect

As mentioned in sections 3.1 and 3.2, there is a concrete asymmetry effect observed in almost all non-isothermal experiments. The rate of advancement of the heavy fluid finger is higher than that of the light one. It is now interesting to investigate what mechanism is physically causing this asymmetry. Let us first see how the flow picture is altered when using different pair of fluids than the water-based ones shown previously. In order to address this, we first decided to increase the viscosity of our water-based solutions using a small amount of xanthan powder. By adding 195 and 245 mg/L of xanthan powder equally

to heavy and light fluids one may reach the viscosities $\hat{\mu} = 2\times10^{-3}, 5\times10^{-3}$ Pa.s respectively at room temperature. Upon rheological characterization (using HR-3 Discovery Hybrid rheometer from TA Instruments) it is found that the shear-thinning effects associated with addition of xanthan gum are negligible for the concentration given and our range of shear rate ($\hat{\dot{\gamma}} = [0,3]$ 1/s).

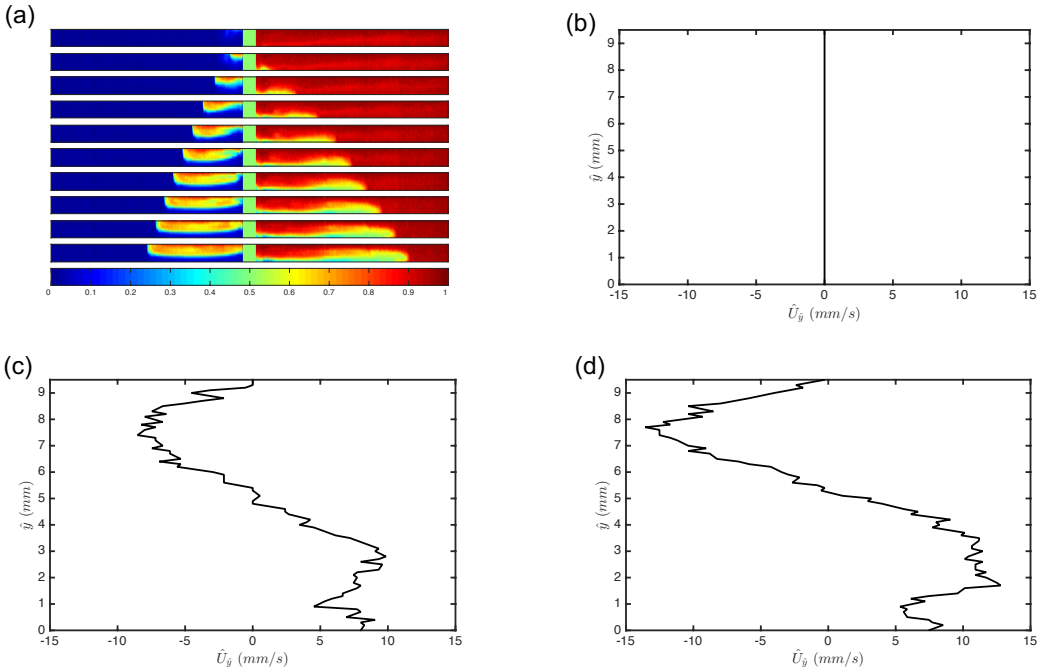

Figure 9. (a) Snapshots of non-isothermal study. The representative Ultrasound Doppler Velocimetry (UDV) profiles are plotted in parts b-d. (b) velocity profile over $\hat{t} = [0,4.0]s$, (c) velocity profile over $\hat{t} = [14.6,\ 18.6]s$, (d) velocity profile over $\hat{t} = [21.0,25.0]s$.

Figure 10(a) shows snapshots of non-isothermal experiments carried using high-viscosity water solutions for lower concentration of xanthan (195mg/L) at $\hat{t}$ = 30 s, At = 0.0035 and various inclination angles, β. Note that the Prandtl number, Pr, is almost doubled in this case compared to our previous non-isothermal examples shown in **Fig. 4(b)**. First thing to note is that the flow is much decelerated due to the higher viscosity of the fluids. Note that for higher concentration of xanthan corresponding to $\hat{\mu} = 5\times10^{-3}3$ Pa.s this deceleration is even more pronounced (results not shown here for brevity). From **Fig.**

10(a) we can interestingly still observe the signs of asymmetry in the case of high-viscosity water solution as well; see for instance β = 0° and 30° cases. Altering the Prandtl number, $Pr = \hat{v}/\hat{\alpha}$, may be achieved through changing either the viscosity (that we just explored) or thermal diffusivity. In order to change the latter we shall choose a fluid with different thermal conductivity, κˆ, than that of water. Glycerine-water solutions were selected for this purpose (20 and 50% weight for $\hat{\mu} = 2\times10^{-3}, 5\times10^{-3}$ Pa.s respectively).Note that $\hat{\kappa}_{gly} \approx 0.47\hat{\kappa}_{wat}$. so we can explore an even larger range of Pr through this experiment. **Figure 10(b)** shows snapshots of experiment run using 20% glycerine-water solution. Compared to the high-viscosity water case we can see that the fingers propagate faster. The asymmetric behavior, however, still persists over a large range of inclination angles. Similar findings were observed for 50% glycerine-water solution (results not shown here for brevity).

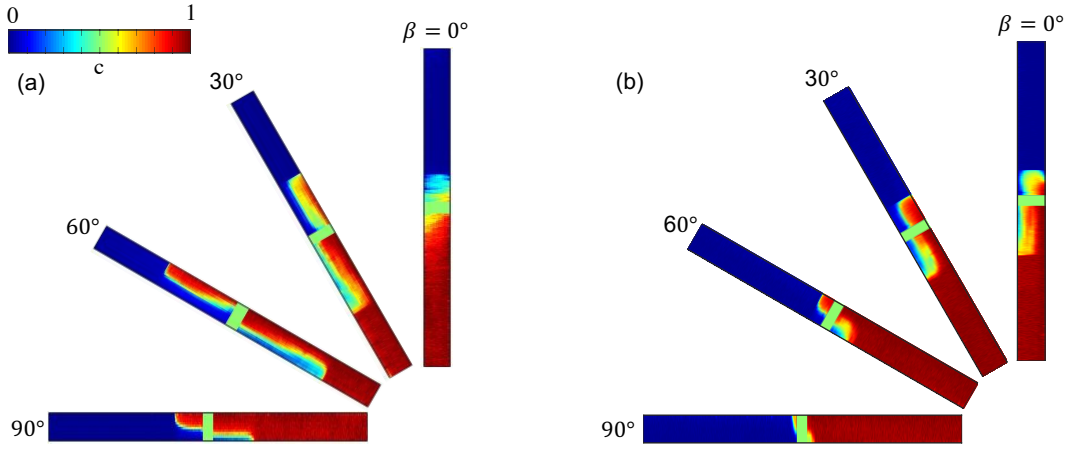

Figure 10. Snapshots of experiments for non-isothermal exchange flow for (a) Glycerol-water solution with $\hat{T}_{H,0} = 25$ ℃, $\hat{T}_{L,0} = 49$ ℃, $\hat{\rho}_{H,0} = 1045\ Kg/m^3$, $\hat{\rho}_{L,0} = 1037.7\ Kg/m^3$, $\hat{\mu}_{H,0} = 0.002\ Pa.s$, $\hat{\mu}_{L,0} = 9.5\times10^{-4}\ Pa.s$, at time $\hat{t} = 30.0\ s$. (b) Xanthan-water solution with$\hat{T}_{H,0} = 25$ ℃, $\hat{T}_{L,0} = 45.4$ ℃, $\hat{\rho}_{H,0} = 997.05Kg/m^3$, $\hat{\rho}_{L,0} = 990.1Kg/m^3$, $\hat{\mu}_{H,0} = 0.002\ Pa.s$, $\hat{\mu}_{L,0} = 5.9\times 10^{-4}\ Pa.s$, at time $\hat{t} = 30.0\ s$.

So far, we have spotted flow asymmetry over a wide range of inclination angles, density differences and even fluid pairs. However, it is still unclear what is causing this effect. Let us have a fundamental look into the non-isothermal problem in hand. From the Navier-Stokes momentum equations and in the absence of an imposed pressure gradient, the fluid inertia dictating the velocity field and flow dynamics will be an outcome of resultant buoyant and viscous stresses. The temperature does not appear directly into the momentum equations but, in the Boussinesq limit, may modify the buoyant and viscous stresses meaning the fluids density and viscosity field. Keeping our density differences in non-isothermal tests the same as those of symmetric isothermal experiments, we basically have the same driving buoyant stress. The only other contribution of the temperature might then be on viscosity. The heavy cold fluid can be more viscous than the light hot one due to the dependence of the viscosity on temperature; see Eq. (1). It could be that the asymmetry is being caused due to such viscosity stratification. If this hypothesis is correct we shall observe an approximately asymmetric flow in an isothermal case where the heavy fluid is more viscous than the light one. In order to check this, we designed an isothermal experiment where the xanthan powder (195 mg/L creating $\hat{\mu}_H = 2\times10^{-3}$Pa.s) was only added to the heavy fluid densified by sodium chloride, NaCl. **Figure 11** shows snapshots of such experiment at various inclination angles. Note that the density difference is kept the same as the one in **Fig. 4** (At = 0.01) to make a direct comparison with non-isothermal case feasible. It is interestingly observed that the flow is mostly symmetric in this case suggesting that the viscosity ratio between the fluids cannot be the cause of the asymmetry. We even checked using a more extreme viscosity ratio (245 mg/L of xanthan creating $\hat{\mu}_H = 5\times10^{-3}$ Pa.s) however the flow was still symmetric (results not shown here for

brevity). Our hypothesis on the formation of asymmetry due to viscosity contrast was proven wrong from the test in **Fig. 11**. The critical question still remains: What is really causing the asymmetry? Let us not be mistaken, the contribution of temperature still has to come through fluids density and/or viscosity modification.

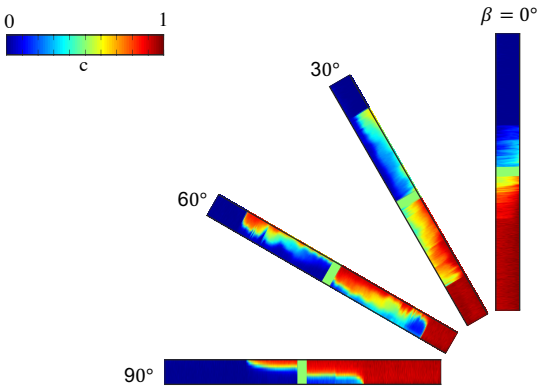

Figure 11. Xanthan-1side. Snapshots of experiments for isothermal exchange flow with Xanthan added to heavy (salt-water) fluid with $\hat{\rho}_{H,0} = 1017.7\ Kg/m^3$, $\hat{\rho}_{L,0} = 997.5\ Kg/m^3$, $\hat{\mu}_{H,0} = 0.002\ Pa.s$, $\hat{\mu}_{L,0} = 8{\times}10^{-4}\ Pa.s$, at time $\hat{t} = 30.0\ s$. $(At = 0.01,\ Re = 146.86\ , m = 0.4,\ Pr = 0.0144,\ Pe = 291506)$The field of view is $2000{\times}9.525\ mm^2$.

We earlier discussed that the former cannot be the reason. What about the latter? Have we thoroughly investigated the viscosity modification effects? Throughout the course of this research we thought about the possibility of interaction of fluids with solid boundary (polycarbonate tube) and their possible effect on flow asymmetry. In section II we discussed in detail how the heat transfers within the solid pipe in all three radial, circumferential and axial directions has been minimized for an adiabatic flow assumption to be valid. It is safe to assume that the asymmetry is not being caused due to the heat transfer within the solid pipe. But what about the heat exchange between the solid and

fluids? This is something that we have not explored yet. Prior to each non-isothermal experiment, the two sides of the pipe are filled with hot and cold fluids. It is reasonable to assume the solid pipe thus reaches a temperature equilibrium with fluids on each side. Upon opening the gate valve and the release of the flow, the heavy cold fluid finger advances through the pipe which is at a higher temperature. During this phase, heat can be transferred from the hot solid wall to the heavy cold finger warming it locally. We may postulate that the viscosity of the heavy fluid region in contact with the solid wall can drop below that of the cold bulk flow. This low-viscosity film region may then act to lubricate the bulk finger which is cold and heavy. Upon a deeper look into the literature, in fact, we did find similar lubricating effects due to wall heating; see for instance [98] for non-isothermal pressure-driven displacement flows in 2D channels. In order to back this hypothesis up we designed one last experiment! Keeping the density configuration unstable (heavy fluid being released into the light one) we tried to add heat to the heavy fluid this time rather than the light one. Of course by adding heat the density of the fluid drops. In order to keep the density of the hot fluid higher than the light one, we densified this phase using salt (sodium chloride, NaCl). In other words, in this case we add both salinity and heat to the heavy phase which introduces Double Diffusive (DD) effects. If our hypothesis is correct, since in this configuration the cold fluid advances upward (instead of downward in non-isothermal case) coming into contact with the hot wall, we shall expect to see the asymmetry in the opposite direction. In other words, this time the light finger should advance faster than the heavy one.

Figure 12(a) shows experimental snapshots of the flow when hot saline water is being released into the cold fresh one at $\beta = 60°$. Again, the density difference is kept the

same as the one in **Fig. 4** to make a direct comparison with previous cases feasible. We interestingly observe that the light finger advances faster than the heavy one, solidifying our lubricating film hypothesis. **Figure 12(b)** suggests that such opposite asymmetry effect can roughly be observed over other inclination angles as well. Note that due to the entirely different dynamics of the flow, we are not expecting to observe the same degree of asymmetry in the test case shown (**Fig. 12**) compared to the previous non-isothermal results (for instance **Fig. 4(b)**). As can be seen in **Fig. 12(b)**, the interfacial instabilities of the given DD flow are completely different than those presented before for non-isothermal case in the absence of added salinity. Understanding the behavior of such complex flows require further research and is beyond the scope of current work. We aim to address these in our future works.

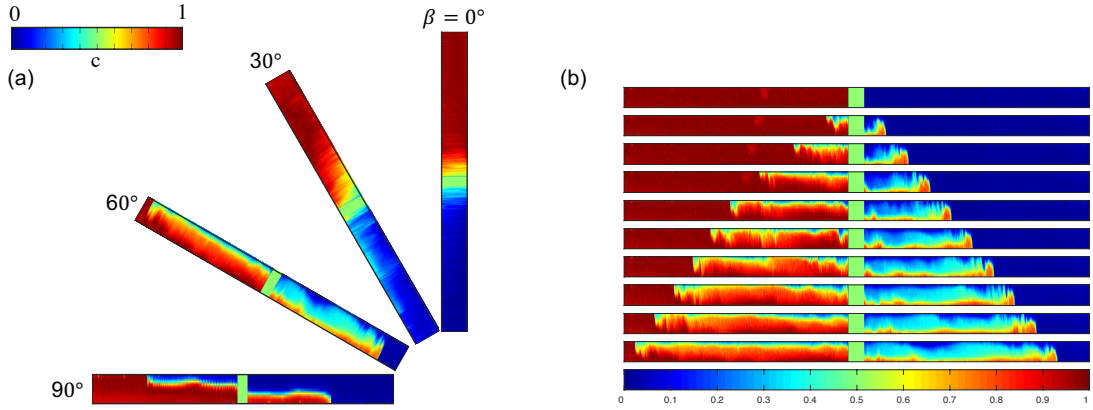

Figure 12. Snapshots of experiments for double diffusion exchange flow with salt added to hot water. $\hat{T}_{H,0} = 25$ ℃, $\hat{T}_{L,0} = 59$℃, $\hat{\rho}_{H,0} = 1017.14\ Kg/m^3$, $\hat{\rho}_{L,0} = 997\ Kg/m^3$, $\hat{\mu}_{H,0} = 4.7\times10^{-4} Pa.s$, $\hat{\mu}_{L,0} = 8\times10^{-4}\ Pa.s$ $\left(At = 0.01,\ Re = 633.6, m = 0.59, Pr = 33\times10^{-4},\ Pe = 291506\right)$ (a) Change in flow by inclination angle, β, at time $\hat{t} = 30.0\ s$.

3.4 Asymmetry quantification

The asymmetry in advancing heavy and light fluid fingers was found to be a prevalent feature of almost all non-isothermal and double diffusive buoyancy-driven

exchange flows as discussed in the previous sections. It would be useful to quantify the asymmetry level over all full range of experiments. Here, we have defined a dimensionless asymmetry parameter, e, as

$$e = (\hat{V}_{f,H} - \hat{V}_{f,L})/\hat{V}_t \,. \tag{4}$$

The asymmetry parameter, e, has been plotted in **Fig. 13** versus inclination angle, β, for various isothermal and non-isothermal experiments. There are a few interesting observations we can make from such dimensionless representation. First, note that the e ≈ 0 for isothermal experiments, suggesting a symmetric flow as also noted in previous findings of Seon et al. [14– 16, 45, 22]. The level of asymmetry is higher for non-isothermal experiments. Asymmetries of up to 50% may be spotted for such cases. The highest dimensionless asymmetry occurs over an intermediate range of inclination angle (10° ≤ β≤ 45°). Lastly, it can be interestingly observed that the asymmetry curves roughly collapse into one for various Atwood numbers (at least in the non-isothermal case).

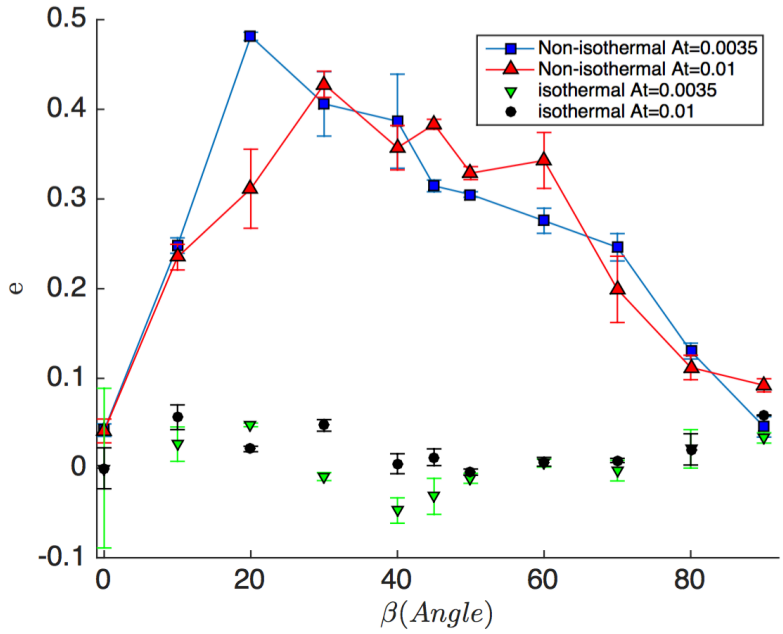

Figure 13. Change in asymmetry with inclination angle for Non-isothermal study versus isothermal

4. Discussion and future works

In this work, we have experimentally studied the Buoyancy-driven exchange flow of two Newtonian fluids in an inclined pipe in the presence of temperature difference between the fluids i.e. non-isothermal. First in the isothermal limit, detailed benchmarking tests were made upon the established exchange flow studies of [15, 16, 17, 45] and an excellent agreement both qualitatively and quantitatively have been achieved in flow classification, frontal velocity and macroscopic diffusion coefficient. Then non-isothermal case was studied where the buoyancy force drives cold heavy fluid into the hot light one in an adiabatic pipe with small aspect ratio. A wide range of the governing dimensional and dimensionless parameter spaces, not covered before in any experimental study have been covered in our experiments where Boussinesq approximation holds because of the choice of low Atwood numbers. *Viscous* regimes are found at near-horizontal inclination angles and as the pipe is progressively inclined towards vertical the *intermittent* and *fully diffusive* regimes are observed where the degree of flow instability and mixing enhances. The maximum interpenetration rate of heavy and light fluids in both isothermal and non-isothermal cases is found to occur at an intermediate inclination angle, reminiscent to the well-known Boycott effect [47].

In the non-isothermal case, the fluids temperature difference is found to significantly increase the flow instability and mass diffusion across the interface which can be of extreme importance in designing counter-current extraction columns processes where the goal is to maximize the mixing between the two phases [6]. For the first time we have observed a novel asymmetric behavior in the non-isothermal flows where interestingly a light hot finger propagates slower than heavy cold finger for both water and water-glycerin

solutions. This asymmetricity in flow behavior never has been observed before in the isothermal limit. Difference in bulk viscosity of heavy and light fluids due to temperature difference was first thought to be the reason of this phenomenon. However, obtained results from more additional set of experiments, where more-viscous heavy xanthan-water interpenetrates a less-viscous light water solution in the isothermal limit revealing symmetric flows, suggest that bulk viscosity contrast between the two fluids may not cause the flow asymmetry. The asymmetric behavior is then hypothetically attributed to the wall contact and the formation of a warm less-viscous *film* of the fluid *lubricating* the cold more-viscous finger along the pipe. On the other side of the pipe, a cool more-viscous film forms *decelerating* the hot less-viscous finger. Further supplementary experiments were precisely-designed in which the heat was added to the heavy fluid densified by salt in order to clarify the root of this phenomenon. It was interestingly observed that the hot finger advances slower than the cold one, further solidifying the lubricating film hypothesis. We additionally investigated the double diffusive effects associated with the diffusion of mass (salinity) and heat where for the same range of density differences, the level of flow asymmetry is found to decrease. We eventually quantified the asymmetric behavior of the flow over the full range of non-isothermal experiments carried.

As future work, by using the Infrared (IR) approach we are planning to implement real-time measurements of the temperature field (thermography) in our experiments to visualize the concentration and thermal fields simultaneously in the exchange flow. An IR camera with spectral range of 1.5-5 μm and spatial resolution of 30 μm, and appropriate optically transparent and thermally insulator materials for main tube and vacuum box will be used accordingly. A polymer called Ethylene tetrafluoroethylene (ETFE) may

potentially be a good future candidate for this purpose due to its high transmissivity of ~90% in the spectral range of 0.2-2.5 μm and relatively low thermal conductivity of 0.238 $W/(m.K)$. The intergraded flow visualization and thermography enable us to: (1) understand the fundamental double-diffusive effects underlying the flow [49] by revealling how closely the temperature and concentration (salinity) fronts follow one another during the evolution of the flow and (2) better clarify the nature of the lubricating layers forming underneath the cold finger due to wall contact. Remarkable insight into such the fundamental problem of convective flows in inclined settings can be achieved by the results presented along with future research directions laid out.

References

[1] J. Whitehead and K. Helfrich, “Instability of flow with temperature-dependent viscosity: A model of magma dynamics,” *J. Geophys. Res*., vol. 96, no. B3, pp. 4145–4155, 1991.

[2] J. Simpson, *Gravity Currents in the Environment and the Laboratory*. Cambridge University Press, Cambridge, 2nd ed., 1997.

[3] J. Shin, S. Dalziel, and P. Linden, “Gravity currents produced by lock exchange,” *J. Fluid Mech*., vol. 521, pp. 1–34, 2004.

[4] V. Birman, J. Martin, E. Meiburg, and P. Linden, “The non- Boussinesq lock-exchange problem. Part 2. High- resolution simulations,” *J. Fluid Mech*., vol. 537, pp. 125–144, 2005.

[5] H. Pratt and M. Baird, “Axial dispersion,” 1983.

[6] W. Chantry, R. Berg, and H. Wiegandt, “Application of pulsation to liquid-liquid extraction,” *Ind. Eng. Chem*., vol. 47, no. 6, pp. 1153–1159, 1955.

[7] D. Ruthven and C. Ching, “Counter-current and simulated counter-current adsorption separation processes,” *Chem. Eng. Sci*., vol. 44, no. 5, pp. 1011–1038, 1989.

[8] P. Schweitzer, *Handbook of separation techniques for chemical engineers*. McGraw-Hill New York etc., 1988.

[9] S. Birajdar, S. Rajagopalan, J. Sawant, and S. Padmanabhan, “Continuous countercurrent liquid–liquid extraction method for the separation of 2, 3-butanediol from fermentation broth using n-butanol and phosphate salt,” *Process Biochem*., vol. 50, no. 9, pp. 1449–1458, 2015.

[10] R. Rao, M. Talluri, T. Krishna, and K. Ravindranath, "Continuous counter current extraction, isolation and determination of solanesol in Nicotiana tobacum L. by non-aqueous reversed phase high performance liquid chromatography," *J. Pharm. Biomed. Anal*., vol. 46, no. 2, pp. 310–315, 2008.

[11] T. Cunha and R. Aires-Barros, "Large-scale extraction of proteins," *Mol. Biotechnol*., vol. 20, no. 1, pp. 29–40, 2002.

[12] M. Baird, K. Aravamudan, N. Rao, J. Chadam, and A. Peirce, "Unsteady axial mixing by natural convection in vertical column," *AIChE J*., vol. 38, p. 1825, 1992.

[13] M. Debacq, V. Fanguet, J. Hulin, D. Salin, and B. Perrin, "Self similar concentration profiles in buoyant mixing of miscible fluids in a vertical tube," *Phys. Fluids*, vol. 13, pp. 3097–3100, 2001.

[14] M. Debacq, J. Hulin, D. Salin, B. Perrin, and E. Hinch, "Buoyant mixing of miscible fluids of varying viscosities in vertical tube," *Phys. Fluids*, vol. 15, pp. 3846–3855, 2003.

[15] T. Seon, J.-P. Hulin, D. Salin, B. Perrin, and E. Hinch, "Buoyant mixing of miscible fluids in tilted tubes," *Phys. Fluids*, vol. 16, pp. 103–106, 2004.

[16] T. Seon, J.-P. Hulin, D. Salin, B. Perrin, and E. Hinch, "Buoyancy driven miscible front dynamics in tilted tubes," *Phys. Fluids*, vol. 17, pp. 031702(1)–(4), 2005.

[17] T. Seon, J.-P. Hulin, D. Salin, B. Perrin, and E. Hinch, "Laser-induced fluorescence measurements of buoyancy driven mixing in tilted tubes," *Phys. Fluids*, vol. 18, pp. 041701(1)–(4), 2006.

[18] Y. Hallez and J. Magnaudet, "Effects of channel geometry on buoyancy-driven mixing," *Phys. Fluids*, vol. 20, pp. 053306(1) – (9), 2008.

[19] K. Sahu and S. Vanka, "A multiphase lattice Boltzmann study of buoyancy-induced mixing in a tilted channel," *Comput. Fluids*, vol. 50, no. 1, pp. 199–215, 2011.

[20] P. Redapangu, S. Vanka, and K. Sahu, "Multiphase lattice Boltzmann simulations of buoyancyinduced flow of two immiscible fluids with different viscosities," *Eur. J. Mech.-B Fluids*, vol. 34, pp. 105–114, 2012.

[21] Y. Hallez and J. Magnaudet, "Buoyancy-induced turbulence in a tilted pipe," *J. Fluid Mech*., vol. 762, pp. 435–477, 2015.

[22] F. Sebilleau, R. Issa, and S. Walker, "Analysis of turbulence modelling approaches to simulate singlephase buoyancy driven counter-current flow in a tilted tube," *Flow Turbul. Combust*., pp. 1–38, 2015.

[23] T. Seon, J. Znaien, D. Salin, J.-P. Hulin, E. Hinch, and B. Perrin, "Transient buoyancy-driven front dynamics in nearly horizontal tubes," *Phys. Fluids*, vol. 19, pp. 123603(1) – (11), 2007.

[24] R. Kerswell, "Exchange flow of two immiscible fluids and the principle of maximum flux," *J. Fluid Mech*., vol. 682, pp. 132–159, 2011.

[25] A. Wakale, K. Venkatasubbaiah, and K. Sahu, "A parametric study of buoyancy-driven flow of twoimmiscible fluids in a differentially heated inclined channel," *Comput. Fluid*s, vol. 117, pp. 54–61, 2015.

[26] O. Reynolds, "An experimental investigation of the circumstances which determine whether the motion of water shall be direct or sinuous, and of the law of resistance in parallel channels.," *Proc. Roy. Soc*., vol. 35, pp. 84–99, 1883.

[27] R. Zhang, X. He, G. Doolen, and S. Chen, "Surface tension effects on two-dimensional two-phase Kelvin–Helmholtz instabilities," *Adv. Water Resour*., vol. 24, no. 3, pp. 461–478, 2001.

[28] H. Yoshikawa and J. Wesfreid, "Oscillatory Kelvin–Helmholtz instability. Part 2. An experiment in fluids with a large viscosity contrast," *J. Fluid Mech*., vol. 675, pp. 249–267, 2011.

[29] S. Dalziel, M. Patterson, C. Caulfield, and I. Coomaraswamy, "Mixing efficiency in high-aspect-ratio Rayleigh-Taylor experiments," *Phys. Fluids*, vol. 20, pp. 065106(1) – (14), 2008.

[30] G. Batchelor and J. Nitsche, "Instability of stationary unbounded stratified fluid," *J. Fluid Mech.*, vol. 227, pp. 357–391, 1991.

[31] G. Homsy, "Viscous fingering in porous media," *Ann. Rev. Fluid Mech*., vol. 19, no. 1, pp. 271–311, 1987.

[32] R. Govindarajan and K. Sahu, "Instabilities in viscosity-stratified flow," *Annu. Rev. Fluid Mech*., vol. 46, pp. 331–353, 2014.

[33] E. Siggia, "High Rayleigh number convection," *Annu. Rev. Fluid Mech*., vol. 26, no. 1, pp. 137–168, 1994.

[34] M. Gibert, H. Pabiou, F. Chilla, and B. Castaing, "High-Rayleigh-number convection in a vertical channel," *Phys. Rev. Lett*., vol. 96, no. 8, p. 084501, 2006.

[35] M. Gibert, H. Pabiou, J. Tisserand, B. Gertjerenken, B. Castaing, and F. Chilla, "Heat convection in a vertical channel: Plumes versus turbulent diffusion," *Phys. Fluids*, vol. 21, no. 3, pp. 035109(1) – (11), 2009. 28

[36] J. Tisserand, M. Creyssels, M. Gibert, B. Castaing, and F. Chilla, "Convection in a vertical channel," *New J. Phys*., vol. 12, no. 7, pp. 075024, 2010.

[37] X. Riedinger, J. Tisserand, F. Seychelles, B. Castaing, and F. Chilla, "Heat transport regimes in an inclined channel," *Phys. Fluids*, vol. 25, no. 1, pp. 015117(1) – (15), 2013.

[38] J. Salort, X. Riedinger, E. Rusaouen, J. Tisserand, F. Seychelles, B. Castaing, and F. Chilla, "Turbulent velocity profiles in a tilted heat pipe," *Phys. Fluids*, vol. 25, no. 10, pp. 105110(1) – (16), 2013.

[39] E. Rusaouen, X. Riedinger, J. Tisserand, F. Seychelles, J. Salort, B. Castaing, and F. Chilla, "Laminar and intermittent flow in a tilted heat pipe," *Eur. Phys. J. E*, vol. 37, no. 1, pp. 1–8, 2014.

[40] J. Koster and K. Nguyen, "Steady natural convection in a double layer of immiscible liquids with density inversion," *Int. J. Heat Mass Tran*., vol. 39, no. 3, pp. 467–478, 1996.

[41] K. Sahu and O. Matar, "Stability of plane channel flow with viscous heating," *J. Fluids Eng*., vol. 132, no. 1, pp. 011202(1) – (7), 2010.

[42] W. Goux, L. Verkruyse, and S. Saltert, "The impact of Rayleigh-Benard convection on NMR pulsed- field-gradient diffusion measurements," *J. Magn. Reson*., vol. 88, no. 3, pp. 609–614, 1990. 30

[43] D. D. Gray and A. Giorgini, "The validity of the Boussinesq approximation for liquids and gases," *Int. J. Heat Mass Tran*., vol. 19, no. 5, pp. 545–551, 1976.

[44] B. Brunone and A. Berni, "Wall Shear Stress in Transient Turbulent Pipe Flow by Local Velocity Measurement," *J. Hydraul. Eng-ASCE*, vol. 136, pp. 716–726, 2010.

[45] T. Seon, J. Znaien, D. Salin, J.-P. Hulin, E. Hinch, and B. Perrin, "Front dynamics and macroscopic diffusion in buoyant mixing in a tilted tube," Phys. Fluids, vol. 19, pp. 125105(1) – (7), 2007.

[46] K. Alba, S. Taghavi, and I. Frigaard, "Miscible density-unstable displacement flows in inclined tube," *Phys. Fluids*, vol. 25, pp. 067101(1) – (21), 2013.

[47] A. Boycott, "Sedimentation of blood corpuscles," *Nature*, vol. 104, p. 532, 1920.